PNAS
www.pnas.org

Supplementary Information for

Distinct Signaling by Insulin and IGF-1 Receptors and Their Extra-and Intra-Cellular Domains

Hirofumi Nagao, Weikang Cai, Nicolai J. Wewer Albrechtsen, Martin Steger, Thiago M. Batista, Hui Pan, Jonathan M. Dreyfuss, Matthias Mann and C. Ronald Kahn*

Corresponding author: C. Ronald Kahn

Email: c.ronald.kahn@joslin.harvard.edu

This PDF file includes:

Supplementary Figures S1 to S8

Supplementary Table S1

Other supplementary materials for this manuscript include the following:

Supplementary Spreadsheet: Unlogged_data of all samples

SI Methods and references

Supplementary Figures

Fig. S1

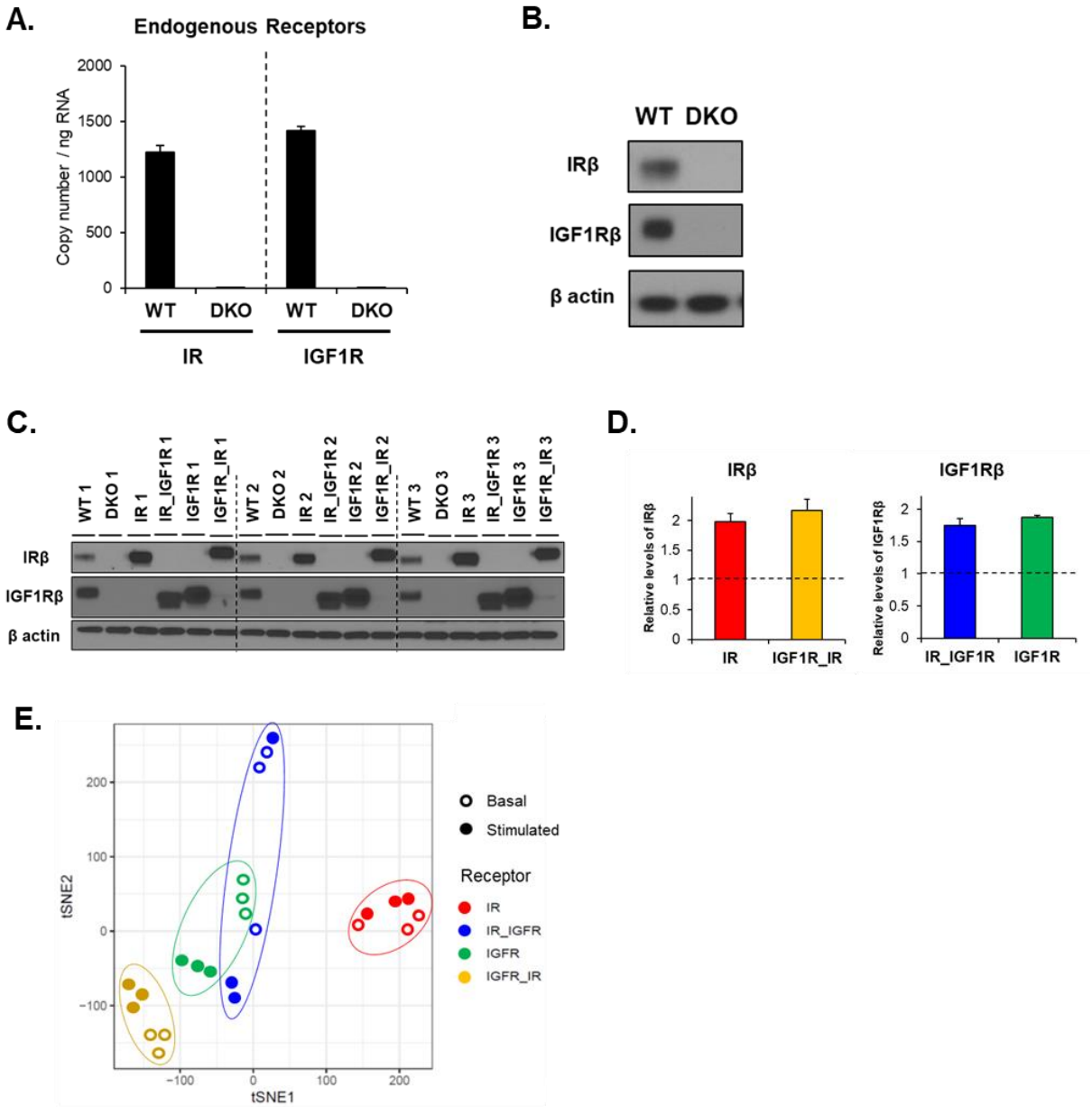

Fig. S1. The Expression of Endogenous IR and IGF1R, and the t-SNE Plots of the Global Phosphoproteomics.

(A) The mRNA levels of endogenous IR and IGF1R from wild-type and DKO brown preadipocytes as determined by qPCR using cDNA standards for quantification. Data are means ± SEM copy number per ng total RNA, n = 3. **(B)** Immunoblotting of IR and IGF1R using antibodies specific for IRβ and IGF1Rβ in lysates from wild-type and DKO cells. **(C and D)** Immunoblot analysis of WT cells, DKO cells and three biological replicates of IR, IR_IGF1R, IGF1R and IGF1R_IR cells for IRβ, IGF1Rβ and β-actin **(C)** and quantification of IRβ and IGF1Rβ **(D)**. The level of each protein in WT cells was set at 1. Data are means ± SEM (n = 3 per group). **(E)** T-distributed Stochastic Neighbor Embedding (t-SNE) of the phosphosites identified by LC-MS/MS of DKO preadipocytes reconstituted with IR, IGF1R, and chimeric receptors IR_IGF1R and IGF1R_IR cells in the basal and hormone stimulated states.

Fig. S2

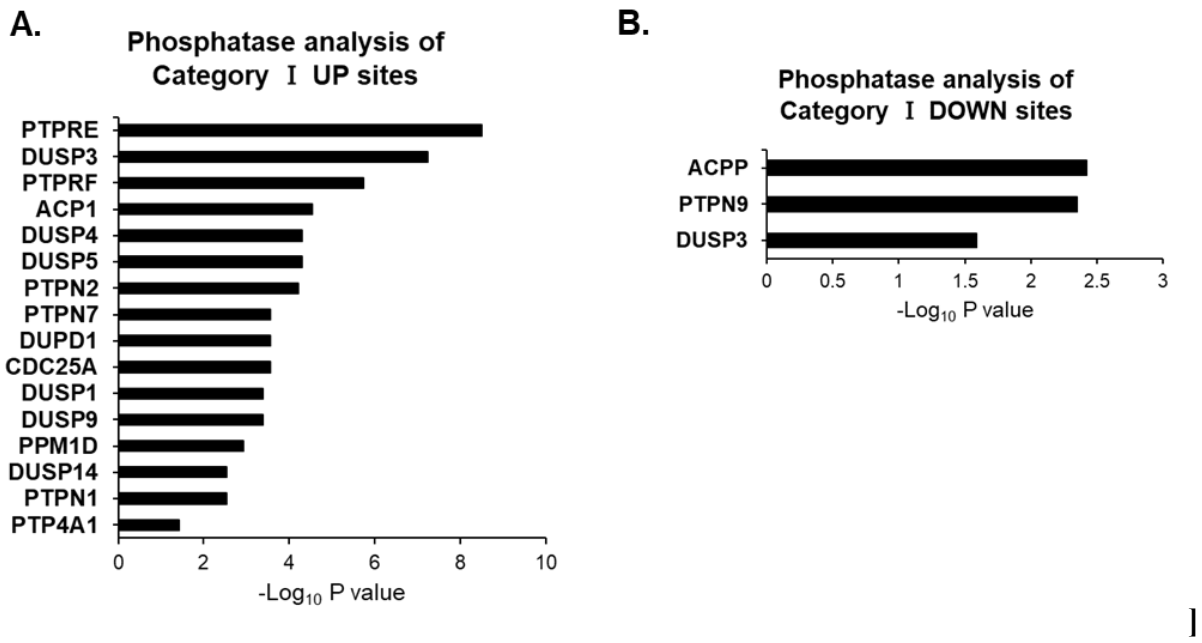

Fig. S2. Phosphatase enrichment analysis for phosphosites in Category I.
(A and B) Phosphatase enrichment analysis for phosphosites in Category IA **(A)** and Category IB **(B)** by using DEPOD (human DEPhOsphorylation Database). Plots are –log10 transforms of enrichment P value.

Fig. S3

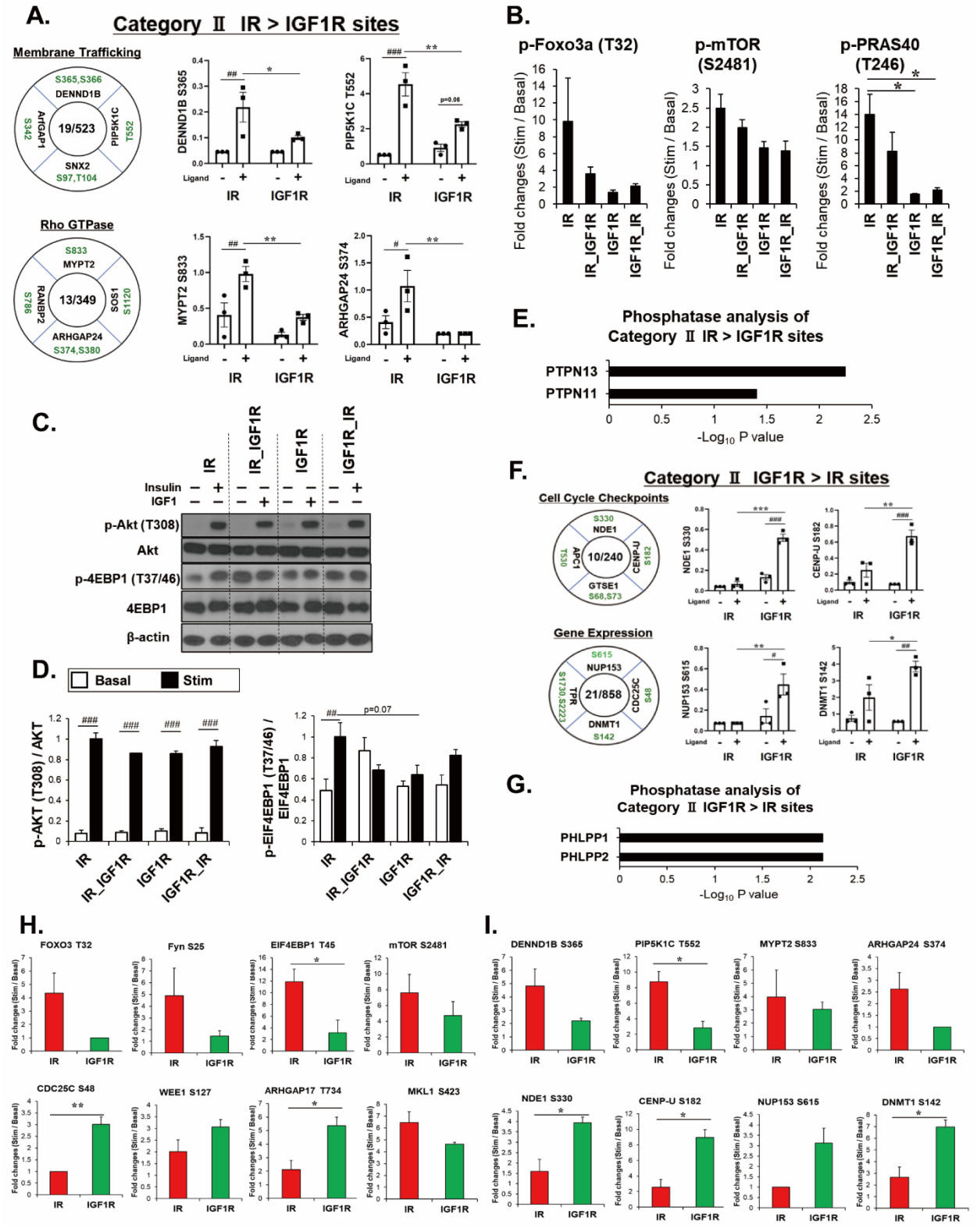
A.
Category Ⅱ IR > IGF1R sites
Membrane Trafficking
S365,S366
DENND1B
ArfGAP1
S342
19/523
PIP5K1C
T552
SNX2
S97,T104
DENND1B S365
PIP5K1C T552
p=0.06
Ligand
IR
IGF1R
Rho GTPase
S833
MYPT2
RANBP2
S786
13/349
SOS1
S1120
ARHGAP24
S374,S380
MYPT2 S833
ARHGAP24 S374
B.
p-Foxo3a (T32)
p-mTOR (S2481)
p-PRAS40 (T246)
Fold changes (Stim / Basal)
IR
IR_IGF1R
IGF1R
IGF1R_IR
C.
Insulin
IGF1
p-Akt (T308)
Akt
p-4EBP1 (T37/46)
4EBP1
β-actin
D.
Basal
Stim
p-AKT (T308) / AKT
p-EIF4EBP1 (T37/46) / EIF4EBP1
p=0.07
E.
Phosphatase analysis of Category Ⅱ IR > IGF1R sites
PTPN13
PTPN11
-Log10 P value
F.
Category Ⅱ IGF1R > IR sites
Cell Cycle Checkpoints
S330
NDE1
APC1
T530
10/240
CENP-U
S182
GTSE1
S68,S73
NDE1 S330
CENP-U S182
Gene Expression
S615
NUP153
TPR
S1720,S2221
21/858
CDC25C
S48
DNMT1
S142
NUP153 S615
DNMT1 S142
G.
Phosphatase analysis of Category Ⅱ IGF1R > IR sites
PHLPP1
PHLPP2
-Log10 P value
H.
FOXO3 T32
Fyn S25
EIF4EBP1 T45
mTOR S2481
CDC25C S48
WEE1 S127
ARHGAP17 T734
MKL1 S423
I.
DENND1B S365
PIP5K1C T552
MYPT2 S833
ARHGAP24 S374
NDE1 S330
CENP-U S182
NUP153 S615
DNMT1 S142

Fig. S3. Differential phosphorylated patterns by IR and IGF1R in the ligand action.
(A) Representation of some important phosphosites in selected pathways, and quantification of exemplary phosphosites in the cluster of Category IIA. Numbers in the center of each circle indicate number of proteins regulated within each pathway. Data are means ± SEM of phosphosites intensity values. # $P < 0.05$, ## $P < 0.01$, ### $P < 0.001$ basal vs ligand, * $P < 0.05$, ** $P < 0.01$ IR vs IGF1R, Two-way ANOVA. **(B)** The densitometric analysis of stimulated level divided by basal level in phosphorylated proteins in Figure 3D. Data are means ± SEM (n = 3 per group). * $P < 0.05$, One-way ANOVA. **(C and D)** Validation of phosphoproteomics by immunoblot in lysates from IR, IR_IGF1R, IGF1R and IGF1R_IR cells. Representative immunoblot analysis **(C)** and quantification of p-Akt^{T308} and p-4EBP1$^{T37/46}$ **(D)**. The level of each protein in stimulated-IR was set at 1. Data are means ± SEM (n = 3 per group). ## $P < 0.01$, ### $P < 0.001$ basal vs ligand, Two-way ANOVA. **(E)** Phosphatase enrichment analysis for phosphosites in Category IIA. **(F)** Representation of some important phosphosites in selected pathways, and quantification of exemplary phosphosites in the cluster of Category IIB. Data are means ± SEM of phosphosites intensity values. # $P < 0.05$ ## $P < 0.01$ ### $P < 0.001$ basal vs ligand, * $P < 0.05$, ** $P < 0.01$, *** $P < 0.001$ IR vs IGF1R, Two-way ANOVA. **(G)** Phosphatase enrichment analysis for phosphosites in Category IIB. **(H)** Analysis of the stimulated level of phosphorylation divided by basal level in phosphorylation for selected proteins in Figure 3B and G. **(I)** Analysis of stimulated level of phosphorylation divided by basal level of phosphorylation for proteins in Figure S3A and F. Data are means ± SEM (n = 3 per group). * $P < 0.05$, ** $P < 0.01$, One-way ANOVA.

Fig. S4

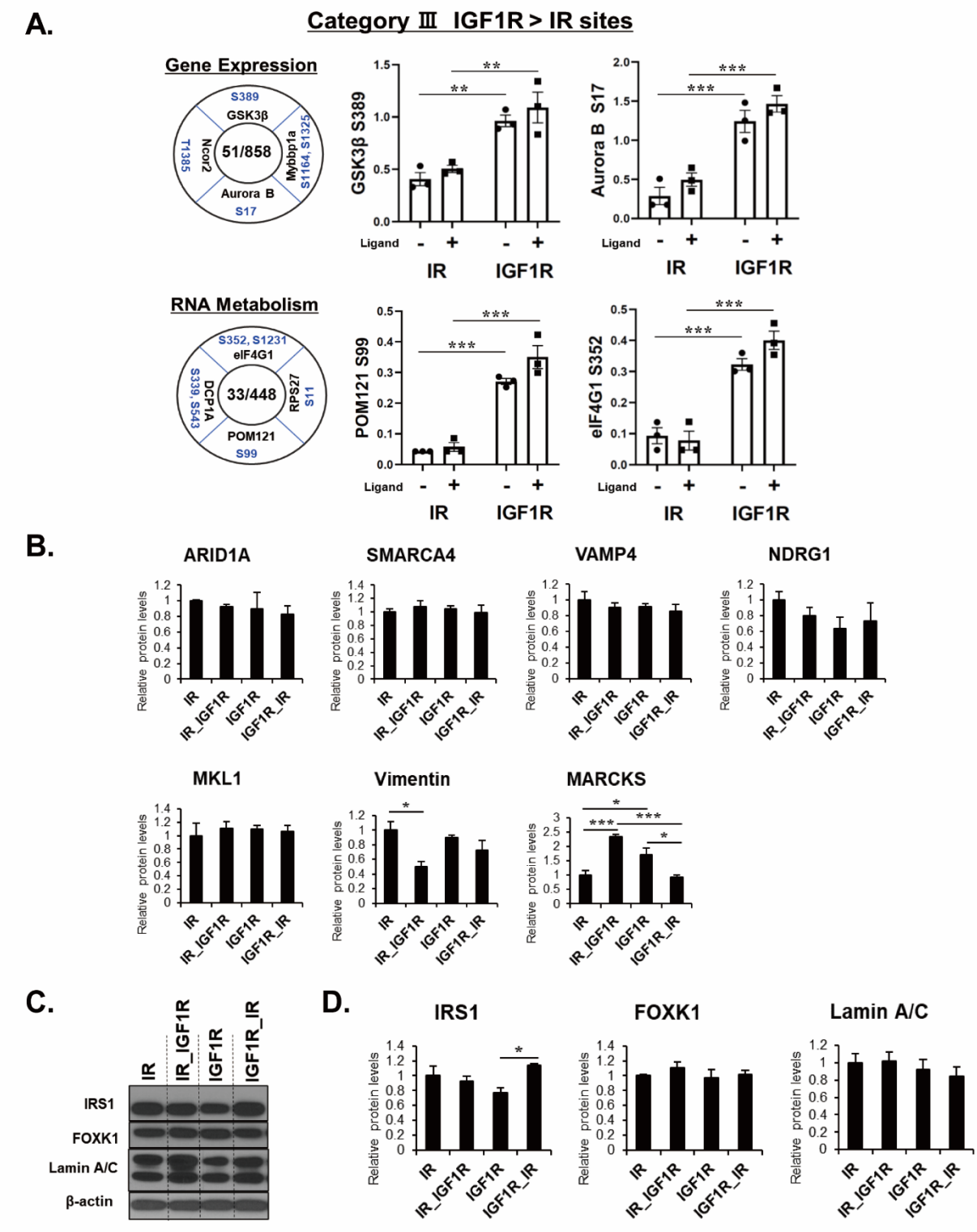
A.
Category Ⅲ IGF1R > IR sites
Gene Expression
S389
GSK3β
51/858
Ncor2
T1385
Mybbp1a
S1164, S1325
Aurora B
S17
GSK3β S389
Aurora B S17
Ligand
IR
IGF1R
RNA Metabolism
S352, S1231
eIF4G1
33/448
DCP1A
S339, S543
RPS27
S11
POM121
S99
POM121 S99
eIF4G1 S352
B.
ARID1A
SMARCA4
VAMP4
NDRG1
MKL1
Vimentin
MARCKS
Relative protein levels
IR
IR_IGF1R
IGF1R
IGF1R_IR
C.
IRS1
FOXK1
Lamin A/C
β-actin
D.
IRS1
FOXK1
Lamin A/C

Fig. S4. Differential phosphorylated patterns by IR and IGF1R in the basal state.
(A) Representation of some important phosphosites in selected pathways, and quantification of exemplary phosphosites in the cluster of Category IIIB. Data are means ± SEM of phosphosites intensity values. ** $P < 0.01$, *** $P < 0.001$ IR vs IGF1R, Two-way ANOVA. **(B)** Densitometric analysis of total proteins in Fig. 5h in lysates from IR, IR_IGF1R, IGF1R and IGF1R_IR cells. The level of each protein in IR was set at 1. Data are means ± SEM (n = 3 per group). * $P < 0.05$ *** $P < 0.001$, One-way ANOVA. **(C and D)** Immunoblotting of total protein levels for IRS1, FOXK1 and Lamin A/C in lysates from cells expressing IR, IR_IGF1R, IGF1R and IGF1R_IR. Representative immunoblot analysis **(C)** and quantification of IRS1, FOXK1 and Lamin A/C **(D)**. The level of each protein in IR was set at 1. Data are means ± SEM (n = 3 per group). * $P < 0.05$, One-way ANOVA.

Fig. S5

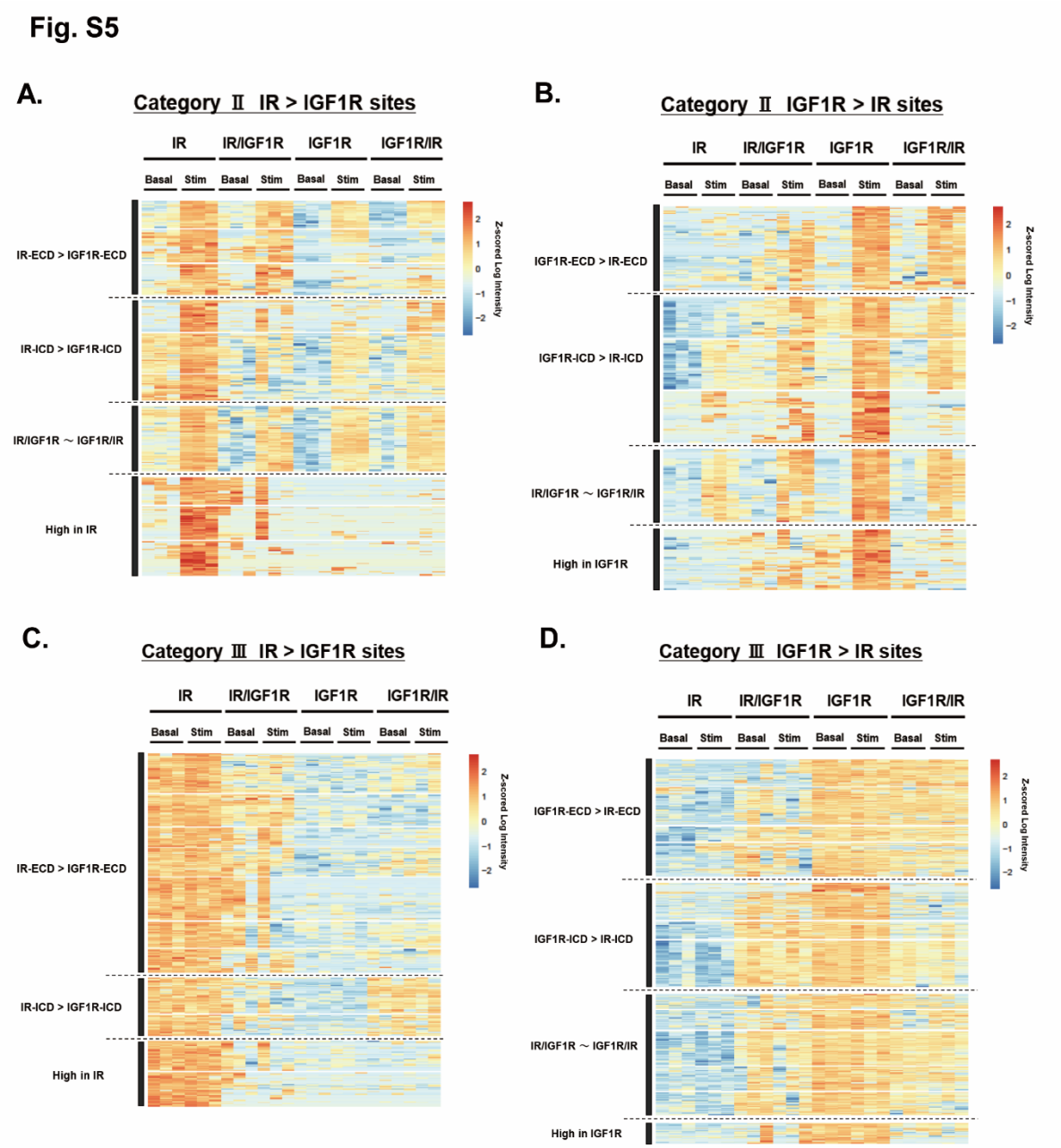

Fig. S5. Domain-dependent effects of IR and IGF1R in the ligand action.

(A-D) A hierarchical clustering map showing sites that were differential between IR vs IGF1R (Fig. 2A) to which has been added the phosphoproteomic data of cells expressing chimeric IR_IGF1R and IGF1R_IR receptors. Then, the cluster of Category IIA **(A)**, the cluster of Category IIB **(B)**, the cluster of Category IIIA **(C)** and the cluster of Category IIIB **(D)** were subclassified to identify the domain-dependency of these phosphosites (FDR < 0.05). Values are Z-scores of log2 transformed intensity values.

Fig. S6

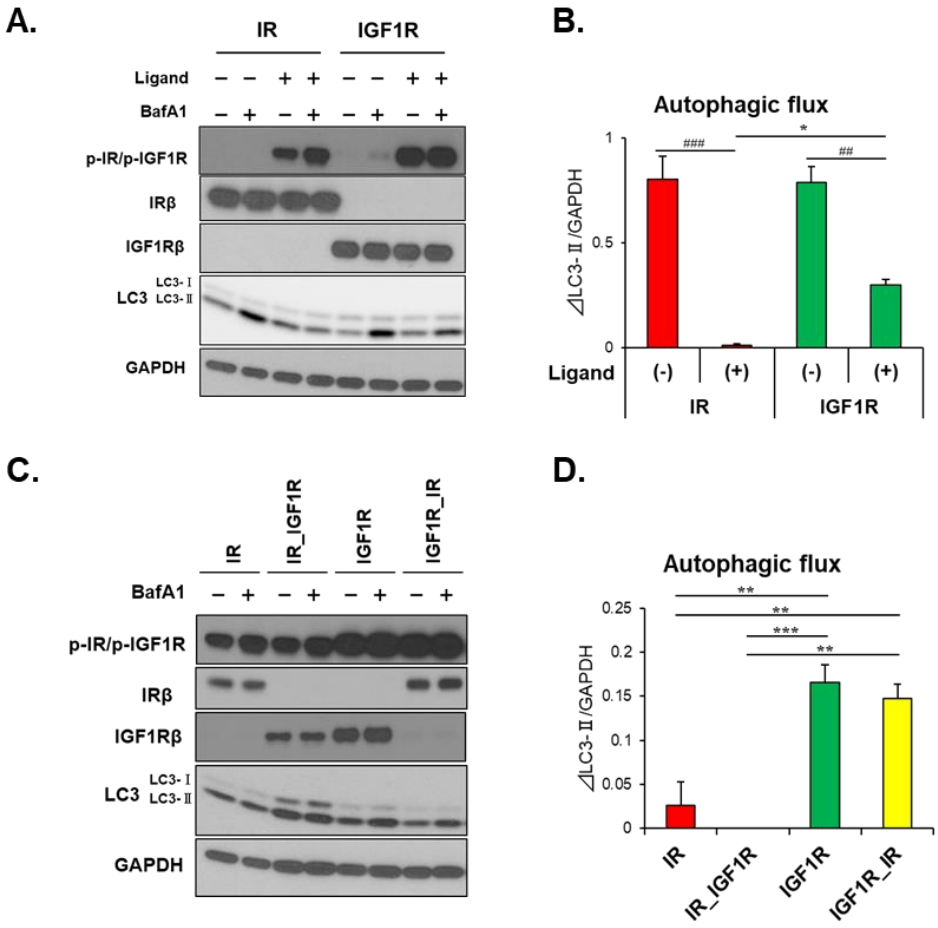

Fig. S6. Changes in autophagic flux in IR, IGF1R and chimeric receptors IR_IGF1R and IGF1R_IR. (A and B) IR and IGF1R cells were cultured for 2 h in FBS- medium with or without 100 μM ligand (insulin for IR and IGF-1 for IGF1R) and 125 nM bafilomycin A1 (BafA1 after 4 h FBS starvation, and then analyzed autophagic flux by immunoblot using anti-LC3 and anti-GAPDH antibodies. Representative western blot analysis for p-IRβ/p-IGF1Rβ, IRβ, IGF1Rβ, LC3 and GAPDH **(A** and quantitative analysis of autophagic flux as measured by ⊿LC3-II with or without BafA1 **(B)** (n = 3 per group). ## P < 0.01, ### P < 0.001 basal vs ligand, * P < 0.05 IR vs IGF1R, Two-way ANOVA. **(C and D)** IR, IGF1R and chimeric receptors IR_IGF1R and IGF1R_IR cells were cultured for 2 h in FBS-medium with 100 μM ligand (insulin for IR and IR_IGF1R, and IGF-1 for IGF1R and IGF1R_IR) and with or without 125 nM Baf.A1 after 4 h FBS starvation, and then analyzed autophagic flux by immunoblot using anti-LC3 and anti-GAPDH antibodies. Representative western blot analysis for p-IRβ/p-IGF1Rβ, IRβ, IGF1Rβ, LC3 and GAPDH **(C)** and quantitative analysis of autophagic flux as measured by ⊿LC3-II with or without BafA1 **(D)** (n = 3 per group). ** P < 0.01, *** P < 0.001, One-way ANOVA.

Fig. S7

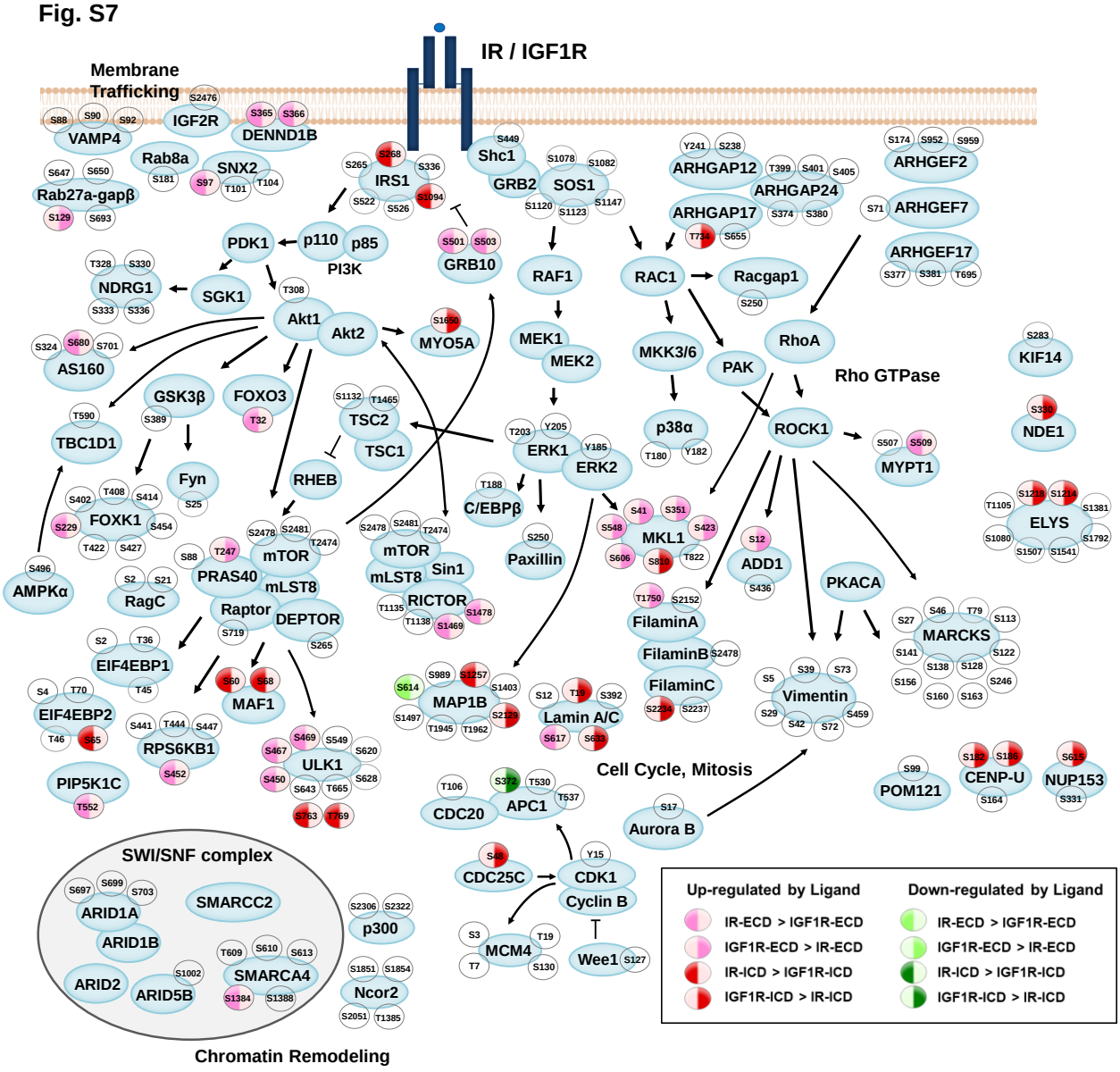
IR / IGF1R
Membrane Trafficking
VAMP4
IGF2R
DENND1B
Rab8a
SNX2
Rab27a-gapβ
IRS1
Shc1
GRB2
SOS1
ARHGAP12
ARHGAP24
ARHGAP17
ARHGEF2
ARHGEF7
ARHGEF17
PDK1
p110
p85
PI3K
GRB10
RAF1
RAC1
Racgap1
NDRG1
SGK1
Akt1
Akt2
MYO5A
MEK1
MEK2
MKK3/6
PAK
RhoA
Rho GTPase
KIF14
NDE1
AS160
GSK3β
FOXO3
TBC1D1
TSC2
TSC1
ERK1
ERK2
p38α
ROCK1
MYPT1
Fyn
RHEB
FOXK1
C/EBPβ
Paxillin
MKL1
ADD1
ELYS
AMPKα
mTOR
mLST8
Sin1
PRAS40
RagC
Raptor
RICTOR
DEPTOR
FilaminA
FilaminB
FilaminC
PKACA
MARCKS
Vimentin
EIF4EBP1
EIF4EBP2
MAF1
MAP1B
Lamin A/C
RPS6KB1
ULK1
PIP5K1C
Cell Cycle, Mitosis
CDC20
APC1
Aurora B
CDC25C
CDK1
Cyclin B
MCM4
Wee1
POM121
CENP-U
NUP153
SWI/SNF complex
ARID1A
ARID1B
ARID2
ARID5B
SMARCC2
SMARCA4
p300
Ncor2
Chromatin Remodeling
Up-regulated by Ligand
IR-ECD > IGF1R-ECD
IGF1R-ECD > IR-ECD
IR-ICD > IGF1R-ICD
IGF1R-ICD > IR-ICD
Down-regulated by Ligand
IR-ECD > IGF1R-ECD
IGF1R-ECD > IR-ECD
IR-ICD > IGF1R-ICD
IGF1R-ICD > IR-ICD

Fig. S7. An integrated phosphorylation map of domain-dependent effects by IR and IGF1R in the stimulated state.

Signaling map showing phosphosites regulated by ligand for IR, IGF1R and chimeric receptors IR_IGF1R and IGF1R_IR identified by phosphoproteomics. Each of the phosphosite indicated was analyzed by Two-way ANOVA ($P < 0.05$). Red-filled circles represent sites for which phosphorylation was increased and green-filled circles sites for which phosphorylation was decreased by ligand. Sites with light red or light green only on left represent sites regulated by IR-ECD greater than IGF1R-ECD. Sites with light red or light green fill only on right represent sites for which regulation was greater by IGF1R-ECD than IR-ECD. Sites with dark red or dark green only on left represent sites regulated by IR-ICD greater than IGF1R-ICD. Sites with dark red or dark green fill only on right represent sites for which regulation was greater by IGF1R-ICD than IR-ICD. Arrows indicate known protein-protein interactions and phosphorylation/dephosphorylation events curated from databases of experimentally defined kinase-substrate relationships (PhosphositePlus) and the literature.

Fig. S8

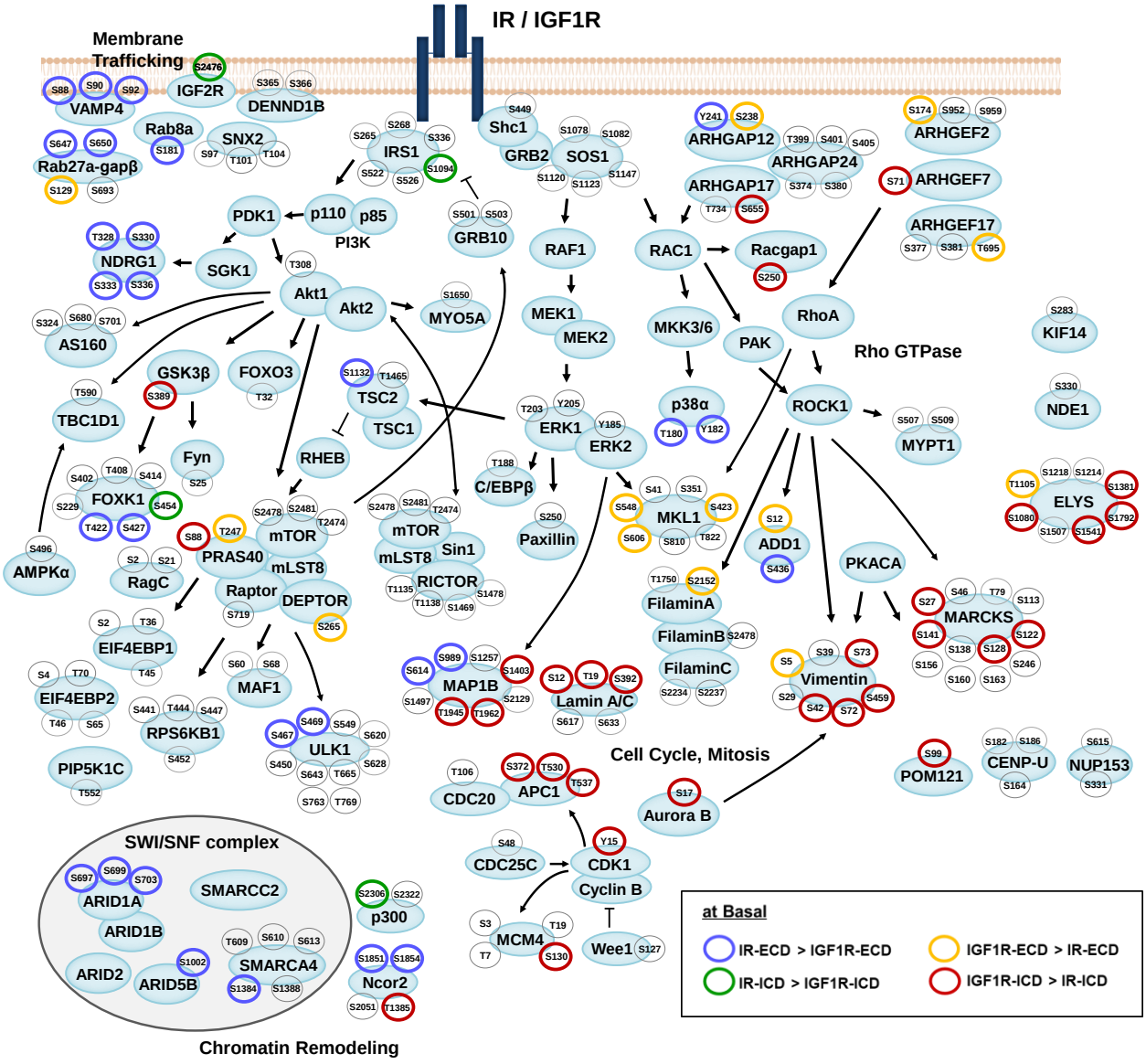
IR / IGF1R
Membrane Trafficking
VAMP4
IGF2R
DENND1B
Rab8a
SNX2
Rab27a-gapβ
IRS1
Shc1
GRB2
SOS1
ARHGAP12
ARHGAP24
ARHGAP17
ARHGEF2
ARHGEF7
ARHGEF17
PDK1
p110
p85
PI3K
GRB10
RAF1
RAC1
Racgap1
NDRG1
SGK1
Akt1
Akt2
MYO5A
MEK1
MEK2
MKK3/6
PAK
RhoA
Rho GTPase
KIF14
NDE1
AS160
GSK3β
FOXO3
TSC2
TSC1
TBC1D1
ERK1
ERK2
p38α
ROCK1
MYPT1
Fyn
RHEB
FOXK1
C/EBPβ
Paxillin
MKL1
ADD1
ELYS
AMPKα
mTOR
PRAS40
mLST8
Sin1
RagC
Raptor
RICTOR
DEPTOR
FilaminA
FilaminB
FilaminC
PKACA
MARCKS
Vimentin
EIF4EBP1
EIF4EBP2
MAF1
RPS6KB1
ULK1
PIP5K1C
MAP1B
Lamin A/C
Cell Cycle, Mitosis
CDC20
APC1
Aurora B
CDC25C
CDK1
Cyclin B
MCM4
Wee1
POM121
CENP-U
NUP153
SWI/SNF complex
ARID1A
ARID1B
ARID2
ARID5B
SMARCC2
SMARCA4
p300
Ncor2
Chromatin Remodeling
at Basal
IR-ECD > IGF1R-ECD
IR-ICD > IGF1R-ICD
IGF1R-ECD > IR-ECD
IGF1R-ICD > IR-ICD

Fig. S8. An integrated phosphorylation map of domain-dependent effects by IR and IGF1R in the basal state.

Signaling cascade map regulated by IR, IGF1R and chimeric receptors IR_IGF1R and IGF1R_IR in the basal state identified by phosphoproteomics. Each of the phosphosite indicated was analyzed by Two-way ANOVA ($P < 0.05$). Blue and green halos represent increased phosphorylation in IR-ECD and IR-ICD in the basal (non-stimulated) state, respectively. Yellow and red halos represent increased phosphorylation in IGF1R-ECD and IGF1R-ICD in the basal state, respectively. Arrows indicate known protein-protein interactions and phosphorylation/dephosphorylation events curated from databases of experimentally defined kinase-substrate relationships (PhosphositePlus) and the literature.

Supplementary Table S1.

The enriched pathways and kinases of all the categories in the heatmap (Fig. 2A).

Category	Description of Cluster	Phospho sites	Proteins	Enriched Reactome Pathways (Top 10)	FDR	Enriched Kinases (Top 10)	P-value
IA	UP by Ligand	446	249	Signaling by NTRK1 (TRKA)	7.88E-07	P38B	3.18E-08
				MAPK targets/ Nuclear events mediated by MAP kinases	1.18E-05	JNK1	4.14E-08
				Gastrin-CREB signalling pathway via PKC and MAPK	1.18E-05	P38A	0.00000133
				Signaling by Rho GTPases	2.12E-05	ERK1	0.0000503
				Signal attenuation	2.12E-05	P70S6KB	0.0000509
				ERK/MAPK targets	2.21E-05	MEK1	0.0000509
				Axon guidance	2.21E-05	PDK1	0.000101
				Signaling by Receptor Tyrosine Kinases	2.21E-05	P70S6K	0.000777
				Cell Cycle	8.08E-05	PLK3	0.000895
				Toll Like Receptor 3 (TLR3) Cascade	8.08E-05	P38G	0.000895
IB	DOWN by Ligand	200	126	None detected		PKCT	0.0459
IIA	UP by Ligand: IR > IGF1R	489	274	mTORC1-mediated signalling	0.0066	mTOR	0.00028
				DCC mediated attractive signaling	0.0066		
				Membrane Trafficking	0.0069		
				PIP3 activates AKT signaling	0.0251		
				Signaling by Rho GTPases	0.033		
				VEGFA-VEGFR2 Pathway	0.0465		
IIB	UP by Ligand: IGF1R > IR	340	248	Cell Cycle, Mitotic	2.05E-05	ERK2	1.64E-09
				M Phase	0.0033	AKT2	0.0393
				Signaling by Rho GTPases	0.0067		
				Mitotic Spindle Checkpoint	0.0183		
				Cell Cycle Checkpoints	0.0356		
				RHO GTPase Effectors	0.0356		
				Gene expression (Transcription)	0.0467		
				G2/M Transition	0.0467		
				Mitotic Prometaphase	0.0467		
				Signaling by MET	0.0467		
IIIA	Altered Basal: IR > IGF1R	636	280	Membrane Trafficking	0.0312	SGK1	0.00862
				Chromatin modifying enzymes	0.0312		
IIIB	Altered Basal: IGF1R > IR	798	497	Cell Cycle	1.39E-11	CDK1	0.000726
				Cell Cycle, Mitotic	1.39E-10	PKACA	0.00699
				M Phase	5.20E-10	PKCT	0.0133
				Signaling by Rho GTPases	9.76E-10	AURB	0.0183
				Gene expression (Transcription)	1.28E-07	CK2A1	0.0301
				Metabolism of RNA	1.00E-06	ERK2	0.0477
				Cell Cycle Checkpoints	2.01E-06		
				Mitotic Spindle Checkpoint	3.07E-06		
				RHO GTPase Effectors	5.66E-06		
				Mitotic Prometaphase	5.66E-06		
IV	Complex Regulation	299	169				

SI Methods

Materials

Antibodies against phospho-IR/IGF-1R (#3024), IRβ (#3025), IGF1Rβ (#3027), β-actin (#4970), p-AKT^{S308} (#4056), AKT pan (#4685), p-FOXO1^{T24}/FOXO3a^{T32} (#9464), FOXO3a (#2497), p-mTOR^{S2481} (#2974), mTOR (#2972), p-4EBP1$^{T37,\ T46}$ (#2855), 4EBP1 (#9452), p-PRAS40^{T246} (#13175), PRAS40 (#2691), MKL1 (#14760), NDRG1 (#5196), Vimentin (#5741), Lamin A/C (#2032), FOXK1 (#12025), ARID1A (#12354), SMARCA4 (#3508), LC3A/B (#12741) and GAPDH (#5174) were purchased from Cell Signaling. Anti-MARCKS antibody (sc-100777) was purchased from Santa Cruz. Anti-Phospho-IRS-1 (Y608) antibody (#09-432) and Anti-IRS-1 antibody (#06-248) were purchased from Millipore. Anti-VAMP4 antibody (#PA1-768) was purchased from Invitrogen. Human insulin was purchased from Sigma and human IGF-1 from Preprotech. Plasmids of IR, IGF1R, and chimeric IR_IGF1R and IGF1R_IR were generated as described previously (*1*). Briefly, mouse IR (MC224356) and IGF1R (MC224342) cDNA clones were purchased from Origene. Normal wild-type IR, IGF1R, chimeric receptors IR_IGF1R (IR extracellular domain (a.a. 1 - 919) fused to IGF1R transmembrane and intracellular domain (a.a. 908 - 1339), numbers excluding signal peptide) and IGF1R_IR (IGF1R extracellular domain (a.a. 1- 907) fused to IR transmembrane and intracellular domain (a.a. 920 - 1345)) were subcloned into pBabe-hygro empty vector. To generate chimeric receptors, an Ile947 to Leu point mutation was introduced into insulin receptor to generate a BclI restriction site using primer pair (5′-ccatcaaatattgccaaactgatcattggacccctcatc-3′; IR Bcll 3: 5′-gatgaggggtccaatgatcagtttggcaatatttgatgg-3′).

Brown preadipocytes isolation and culture

IR/IGF1R double knockout brown preadipocytes were obtained as previously described (*2*). Briefly, preadipocytes were isolated from newborn homozygous IR-lox/IGF1R-lox mice by collagenase digestion of the brown fat pad and immortalized by infection with retrovirus encoding SV40 T-antigen followed by the selection with 2 μg/ml of puromycin. The immortalized preadipocytes were infected with adenovirus expressing GFP alone (to generate control cell lines) or GFP-tagged Cre recombinase (to generate double knockout [DKO] cell lines). GFP-positive cells were sorted and expanded in Dulbecco's Modified Eagle Medium (DMEM) supplemented with 10% heat-inactivated fetal bovine serum (FBS, Atlas Biologicals), 100 U/ml penicillin and 100 μg/ml streptomycin (Gibco) at 37 °C in a 5% CO2 incubator. IR/IGF1R double knock-out preadipocytes were then stably transduced with pBabe retrovirus encoding mouse IR, IGF1R and chimeric receptor IR_IGF1R and IGF1R_IR. Plates (10 cm) of HEK- 293T cells were transiently transfected with 10 μg of pBabe-hygro retroviral expression vectors encoding wild-type or mutant IR or IGF1R sequences and viral packaging vectors SV-E-MLV-env and SV-E-MLV using TransITExpress transfection reagent (Mirus Bio Corp.). 48 h after transfection, virus-containing medium was collected and passed through a 0.45 μm pore size syringe filter. Filter-sterilized Polybrene (hexadimethrine bromide; 12 μg/ml) was added to the virus-loaded medium. This medium was then applied to proliferating (40% confluent) DKO cells. 24 h after infection, cells were treated with trypsin and replated in a medium supplemented with hygromycin (Invitrogen) as a selection antibiotic. Cells were maintained in DMEM with 4.5 g/liter glucose supplemented with 10% FBS, 100 U/ml penicillin and 100 μg/ml streptomycin (Gibco) and cultured at 37°C in a humidified atmosphere of 5% CO2. All animal studies were approved by the Institutional Animal Care and Use Committee (IACUC) at the Joslin Diabetes Center and were in accordance with the National Institutes of Health guidelines.

Immunoblotting

After transfer, polyvinylidene difluoride (PVDF) membranes were blocked in Starting Block T20 solution (Fisher) at room temperature for 1 h, washed 3 times with 1X PBST, and incubated with an appropriate dilution of the primary antibody in Starting Block T20 solution overnight at 4°C. The immunoblots were then washed three times with 1X PBS with Tween-20 (PBST) and incubation with an appropriate dilution of horseradish peroxidase (HRP)-conjugated secondary antibody in Starting Block T20 solution was conducted for additional 1 h. The signals were detected by Immobilon Western Chemiluminescent HRP Substrate (Millipore).

Lysis and digestion for phosphoproteomic analysis

For phosphoproteomics, samples were processed as described previously (*3, 4*). Briefly, cells were seeded so that they were confluent and could be studied at the same time. The confluent cells were washed twice with ice cold PBS, lysed immediately in SDC buffer (4% SDC, 100 mM Tris pH8.5) and snap frozen. Then, the samples were boiled at 95°C for 5 minutes, sonicated for 20 cycles in Biorupter Plus (Diagenode) and then vortexed for 10 seconds. For each sample, 750 µg of protein lysate was alkylated with 10 mM chloroacetamide and reduced with 40 mM tris(2-carboxyethyl)phosphine by incubating for 20 minutes on ice in dark. The samples were then digested with a mixture of LysC protease and trypsin (1:100 ratio) and incubated overnight at 37°C in a ThermoMixer at 1200 rpm.

Phosphopeptide enrichment and LC-MS/MS measurement

Phosphopeptide enrichment was processed as described previously (*4*). Briefly, 750 µl acetonitrile (ACN) and 250µl TK buffer (36% trifluoroacetic acid (TFA) & 3 mM KH2PO4) were added to

the digested peptides, and the samples mixed in a ThermoMixer for 30 seconds at 1,500 rpm. Debris was cleared by centrifugation at 13,000 rpm for 15 min, and the supernatant transferred to 2 ml Deep Well Plates (Eppendorf). TiO2 beads (prepared in 80% ACN, 6% TFA buffer) were added (1:10 ratio protein/beads) and incubated in a ThermoMixer at 40°C and 2000 rpm for 5 min. The TiO2 bound phosphopeptides were then pelleted by centrifugation, transferred to clean tubes and washed 4 times in wash buffer (60% ACN, 1% TFA) to remove nonspecific or non-phosphorylated peptides. The beads were suspended in transfer buffer (80% ACN, 0.5% acetic acid) and transferred on top of single layer C8 Stage Tips and centrifuged until dry. The phosphopeptides were eluted with elution buffer (40% ACN, 20% NH4OH) and concentrated in a SpeedVac for 20 minutes at 45° C. The phosphopeptides were then acidified by addition of 100µl of 1%TFA and loaded on to equilibrated SDBRPS (styrenedivinylbenzene–reversed phase sulfonated, 3M Empore) Stage Tips. The phosphopeptides containing SDBRPS StageTips were washed once in isopropanol/1% TFA and twice with 0.2% TFA. Finally, the desalted phosphopeptides were eluted with 60µl of elution buffer (80% ACN, 1.25% NH4OH). The dried elutes were resuspended in MS loading buffer (3%ACN, 0.3% TFA) and stored at -80°C until LC-MS/MS measurement. LC-MS/MS measurement was performed using Q Exactive HF-X Hybrid Quadrupole-Orbitrap Mass Spectrometer (Thermo Fischer Scientific) coupled online to a nanoflow EASY-nLC1200 HPLC (Thermo Fisher Scientific) as described previously (*4*).

Phosphoproteomic data analysis

Phosphoproteomic data analysis was processed as described previously (*4*). The raw files were processed using Maxquant (*5*) software environment (version 1.5.5.2) with the built in Andromeda search engine for identification and quantification of phosphopeptides. The data were searched

using a target-decoy approach with a reverse database against Uniprot Human reference proteome fasta file with a false discovery rate of 1% at the level of proteins, peptides and modifications using minor changes to the default settings as follows: oxidized methionine, acetylation (protein N-term) and phospho was selected as variable modifications, and carbamidomethyl as fixed modification. A maximum of 2 missed cleavages were allowed, a minimum peptide length of seven amino acids and enzyme specificity was set to trypsin. The Maxquant output phospho table was processed using Perseus (version 1.5.2.11) software suite. For analysis of only the wild-type receptors, phosphopeptides that have at least two valid values were selected, and their missing values were imputed with half of the minimum value of the corresponding phosphopeptide. For analysis of the wild-type and chimeric receptor together, phosphopeptides that have at least 50% valid values were selected, and their missing values were imputed using a random forest algorithm in the R package missForest. All values were further normalized to make all samples have the same median log intensity. The statistical significance of phosphopeptides was assessed with empirical Bayesian linear modeling using the limma package (*6*). P-values were corrected using the Benjamini-Hochberg false discovery rate (FDR). Differences were considered significant when the FDR was <0.05. The top phosphosites that have FDR < 0.05 in the F-tests were selected, then hierarchical cluster analysis was performed based on the Euclidean distance of these selected phosphosites. Gene sets based on canonical pathways (*7*) and human kinase substrates (PhosphositePlus and RegPhos) (*8*) were tested for enrichment analysis using the Fisher exact test. Heatmaps were created with the pheatmap R package.

SI References

1. W. Cai *et al.*, Domain-dependent effects of insulin and IGF-1 receptors on signalling and gene expression. *Nat Commun* **8**, 14892 (2017).
2. J. Boucher *et al.*, A kinase-independent role for unoccupied insulin and IGF-1 receptors in the control of apoptosis. *Sci Signal* **3**, ra87 (2010).
3. S. J. Humphrey, S. B. Azimifar, M. Mann, High-throughput phosphoproteomics reveals in vivo insulin signaling dynamics. *Nat Biotechnol* **33**, 990-995 (2015).
4. T. M. Batista *et al.*, A Cell-Autonomous Signature of Dysregulated Protein Phosphorylation Underlies Muscle Insulin Resistance in Type 2 Diabetes. *Cell Metab **32***, 844-859.e5 (2020).
5. J. Cox, M. Mann, MaxQuant enables high peptide identification rates, individualized p.p.b.-range mass accuracies and proteome-wide protein quantification. *Nat Biotechnol* **26**, 1367-1372 (2008).
6. M. E. Ritchie *et al.*, limma powers differential expression analyses for RNA-sequencing and microarray studies. *Nucleic Acids Res* **43**, e47 (2015).
7. A. Liberzon *et al.*, The Molecular Signatures Database (MSigDB) hallmark gene set collection. *Cell Syst* **1**, 417-425 (2015).
8. A. D. Rouillard *et al.*, The harmonizome: a collection of processed datasets gathered to serve and mine knowledge about genes and proteins. *Database (Oxford)* **2016**, (2016).